

# Gradient-Based Quantitative Photoacoustic Image Reconstruction for Molecular Imaging

B. T. Cox<sup>a</sup>, S. R. Arridge<sup>b</sup> and P. C. Beard<sup>a</sup>

<sup>a</sup> Department of Medical Physics and Bioengineering, University College London,  
Gower Street, London WC1E 6BT, UK  
www.medphys.ucl.ac.uk/research/mle

<sup>b</sup> Department of Computer Science, University College London,  
Gower Street, London WC1E 6BT, UK

## ABSTRACT

The aim in quantitative photoacoustic imaging (QPI) is to recover the spatial distributions of the optical absorption and scattering coefficients from an absorbed energy density distribution (a conventional photoacoustic image). This paper proposes a gradient-based minimisation approach and demonstrates that functional gradients may be calculated efficiently by using a finite element model of light transport based on the diffusion approximation, in conjunction with a related adjoint model. The gradients calculated using this adjoint method are tested against finite-difference estimates, and inversions for the absorption or scattering coefficient distributions (from simulated data) are shown for the case where the other coefficient is known *a priori*. Simultaneous estimation for both absorption and scattering is ill-posed, and so multiwavelength inversion, in which the specific absorption spectra of the constituent chromophores and the wavelength-dependence of the scatter are known, is proposed as a means of ameliorating the ill-posedness. The unknown parameters are now the spatial variation of the chromophore concentrations and scattering coefficient. It is shown that the functional gradients for both of these can be obtained straightforwardly from the gradients for absorption and scatter and require no significant additional calculations. A simulated example is given in which the distributions of two chromophores with different spectra are recovered from absorbed energy images obtained at multiple wavelengths, when the scattering is assumed known.

**Keywords:** photoacoustic imaging, quantitative, functional gradient, absorption coefficient, scattering coefficient, multiwavelength

## 1. QUANTITATIVE PHOTOACOUSTIC IMAGING

In conventional photoacoustic imaging, or photoacoustic tomography (PAT), an image proportional to the absorbed optical energy density is reconstructed from measurements of the acoustic (ultrasonic) waves emitted following the absorption of a short laser pulse. Quantitative photoacoustic imaging (QPI) goes further and recovers the distributions of the optical coefficients - the absorption and scattering coefficients - or chromophore concentrations from this absorbed energy density distribution. This is important because it is the absorption coefficient distribution that is fundamentally related to the tissue morphology and composition. It is the absorption coefficient, and the related chromophore distributions, rather than the absorbed energy that will provide information about tissue functionality. It is not possible, in general, to infer physiological parameters or structure from images of absorbed energy density for two reasons, which may be termed *structural* and *spectral* distortion. An absorbed energy image is not proportional to the underlying absorption coefficient distribution,  $\mu_a$ , but is distorted by the light fluence distribution,  $\Phi$ , which, as it depends on  $\mu_a$  too, makes the absorbed energy a nonlinear function of  $\mu_a$

$$H = \mu_a \Phi(\mu_a, \mu'_s). \quad (1)$$

Furthermore, as the fluence is dependent on the optical wavelength, the absorbed energy spectrum at a given point will not, in general, be proportional to the absorption coefficient spectrum at that point. It is not,

---

Send correspondence to B. T. Cox. [bencox@mpb.ucl.ac.uk](mailto:bencox@mpb.ucl.ac.uk)

Photons Plus Ultrasound: Imaging and Sensing 2007: The Eighth Conference on Biomedical Thermoacoustics, Optoacoustics, and Acousto-optics, edited by Alexander Oraevsky, Lihong V. Wang, Proc. of SPIE Vol. 6437, 64371T, (2007) · 1605-7422/07/\$18 · doi:10.1117/12.700031

therefore, possible to obtain estimates of chromophore concentrations by fitting known specific absorption spectra directly to absorbed energy images obtained at multiple wavelengths.<sup>1</sup>

Cox *et al.*<sup>2,3</sup> presented a QPI algorithm to correct for the effect of the fluence, based on a fixed-point iteration of a finite-element(FE) model of the fluence, which can recover the absorption coefficient distribution exactly when the scattering is known *a priori*. The fluence model was based on the diffusion approximation to the transport equation,

$$(\mu_a + \nabla \cdot \kappa \nabla) \Phi = \text{sources}, \quad (2)$$

where  $\kappa = (3(\mu_a + \mu'_s))^{-1}$ . This equation holds when  $\mu'_s \gg \mu_a$ . The  $\delta$ -Eddington approximation can be used to improve its accuracy close to the surface when the source is a collimated beam.<sup>3-5</sup> This approach, although without the  $\delta$ -Eddington correction, was applied to experimental data by Yuan and Jiang.<sup>6</sup> Ripoll and Ntziachristos<sup>7</sup> also describe an inversion scheme based on the diffusion model, which can recover small perturbations in the absorption coefficient distribution when both the scattering and background absorption coefficients are known.

## 2. GRADIENT-BASED QUANTITATIVE PHOTOACOUSTIC IMAGING

In many situations of practical interest, the scattering distribution will not be known in advance, so to obtain the absorption coefficient distribution accurately, it is necessary to recover both the absorption and scattering coefficients simultaneously from the absorbed energy image. One approach to such an inversion is to minimise the difference between a model of the absorbed energy distribution,  $H(\mu_a, \mu'_s)$ , and a measured image,  $H_{meas}$ . For instance, if the error functional is given by

$$\mathcal{E} = \frac{1}{2} \int (H_{meas} - H(\mu_a, \mu'_s))^2 dV \quad (3)$$

then one way to estimate  $\mu_a$  and  $\mu'_s$  would be to minimise  $\mathcal{E}$ . Consider a cubic PAT image of side 1 cm with cubic voxels of side 100  $\mu\text{m}$ . If the absorption and scattering coefficients within each voxel are to be estimated, then, even for this small example, there are 2 million unknowns. This is a large-scale inverse problem, and the most feasible method of solution is one that makes use of the functional gradients,  $\partial\mathcal{E}/\partial\mu_a$  and  $\partial\mathcal{E}/\partial\mu'_s$ , to inform an iterative minimisation, such as the conjugate-gradient or Broyden-Fletcher-Goldfarb-Shanno (BFGS) methods. In fact, inverting simultaneously for  $\mu_a$  and  $\mu'_s$  distributions is ill-posed and may have nonunique solutions, which makes it difficult to recover  $\mu_a$  and  $\mu'_s$  simultaneously without some additional information. However, the functional gradients for the absorption and scattering coefficients will be useful in the multiwavelength inversion described towards the end of this paper, and so will be introduced here.

### 2.1. Functional Gradient for Absorption Coefficient

Differentiating Eqs. (3) and (1) with respect to  $\mu_a$  at a single point  $\mathbf{x}_0$  gives

$$\frac{\partial\mathcal{E}}{\partial\mu_a} = - \int \frac{\partial H}{\partial\mu_a} (H_{meas} - H) dV \quad (4)$$

and

$$\frac{\partial H}{\partial\mu_a} = \Phi\delta(\mathbf{x} - \mathbf{x}_0) + \mu_a \frac{\partial\Phi}{\partial\mu_a} \quad (5)$$

where  $\delta$  is the Dirac delta function. Substituting Eq. (5) into Eq. (4) gives

$$\frac{\partial\mathcal{E}}{\partial\mu_a} = -\Phi(H_{meas} - H)|_{\mathbf{x}_0} - \int \frac{\partial\Phi}{\partial\mu_a} \mu_a (H_{meas} - H) dV \quad (6)$$

Differentiating Eq. (2) with respect to the absorption coefficient at point  $\mathbf{x}_0$ ,  $\mu_a(\mathbf{x}_0)$ , gives

$$(\mu_a + \nabla \cdot \kappa \nabla) \frac{\partial\Phi}{\partial\mu_a} = -\Phi\delta(\mathbf{x} - \mathbf{x}_0). \quad (7)$$

Now we introduce the adjoint equation with solution  $\Phi^*$ :

$$\boxed{(\mu_a + \nabla \cdot \kappa \nabla) \Phi^* = \mu_a (H_{meas} - H)}. \quad (8)$$

Forming an equation from Eqs. (7) and (8) as follows

$$\Phi^* \times (7) - \frac{\partial \Phi}{\partial \mu_a} \times (8) \quad (9)$$

gives

$$\Phi^* (\mu_a + \nabla \cdot \kappa \nabla) \frac{\partial \Phi}{\partial \mu_a} - \frac{\partial \Phi}{\partial \mu_a} (\mu_a + \nabla \cdot \kappa \nabla) \Phi^* = -\Phi^* \Phi \delta(\mathbf{x} - \mathbf{x}_0) - \frac{\partial \Phi}{\partial \mu_a} \mu_a (H_{meas} - H) \quad (10)$$

By integrating this equation over a volume  $V$  with surface  $S$ , using the identity

$$\int_S ab \nabla c dS = \int_V a \nabla \cdot (b \nabla c) dV + \int_V b \nabla a \cdot \nabla c dV, \quad (11)$$

and noting that both  $\partial \Phi / \partial \mu_a$  and  $\Phi^* \rightarrow 0$  on the boundary  $S$  as  $S \rightarrow \infty$ , the left-hand side of Eq. (10) becomes zero, and so

$$\int \frac{\partial \Phi}{\partial \mu_a} \mu_a (H_{meas} - H) dV = - \int \Phi^* \Phi \delta(\mathbf{x} - \mathbf{x}_0) dV \quad (12)$$

$$= -\Phi^* \Phi |_{\mathbf{x}_0} \quad (13)$$

Substituting this result into Eq. (6) shows that the functional gradient for the absorption coefficient can be written as

$$\boxed{\frac{\partial \mathcal{E}}{\partial \mu_a} = -\Phi (H_{meas} - H) + \Phi \Phi^*} \quad (14)$$

The functional gradient could be calculated using finite differences by perturbing the absorption at every point in the image in turn and noting the effect on the error functional  $\mathcal{E}$ . That would require as many computational runs of the light model as there are voxels, ie. many thousands or millions. By using the adjoint method, on the other hand, the functional gradient can be calculated from just two runs: one of the light model and one of the adjoint model (which is the same basic model but with a different source term). In this particular case, the second term in Eq. (14) will often be small compared to the first and can be neglected. In this situation, the adjoint model is not required at all, as the functional gradient is given simply by  $-\Phi (H_{meas} - H)$ . However, as shown below, the adjoint model is essential for calculating the gradient for  $\mu'_s$ .

## 2.2. Functional Gradient for Scattering Coefficient

In this section, the functional gradient for the diffusion coefficient  $\kappa$  will be obtained in a similar way to that used above, and from that the gradient for  $\mu'_s$  will be calculated. Differentiating Eqs. (3) and (1) with respect to  $\kappa$  at a single point  $\mathbf{x}_0$  gives

$$\frac{\partial \mathcal{E}}{\partial \kappa} = - \int \frac{\partial H}{\partial \kappa} (H_{meas} - H) dV \quad (15)$$

and

$$\frac{\partial H}{\partial \kappa} = \mu_a \frac{\partial \Phi}{\partial \kappa} \quad (16)$$

so

$$\frac{\partial \mathcal{E}}{\partial \kappa} = - \int \frac{\partial \Phi}{\partial \kappa} \mu_a (H_{meas} - H) dV \quad (17)$$

Differentiating Eq. (2) with respect to  $\kappa(\mathbf{x}_0)$  results in

$$(\mu_a + \nabla \cdot \kappa \nabla) \frac{\partial \Phi}{\partial \kappa} = -\nabla \cdot (\delta(\mathbf{x} - \mathbf{x}_0) \nabla \Phi) \quad (18)$$

Forming an equation from Eqs. (18) and (8) as follows

$$\Phi^* \times (18) - \frac{\partial \Phi}{\partial \kappa} \times (8) \quad (19)$$

gives

$$\Phi^* (\mu_a + \nabla \cdot \kappa \nabla) \frac{\partial \Phi}{\partial \kappa} - \frac{\partial \Phi}{\partial \kappa} (\mu_a + \nabla \cdot \kappa \nabla) \Phi^* = -\Phi^* \nabla \cdot (\delta(\mathbf{x} - \mathbf{x}_0) \nabla \Phi) - \frac{\partial \Phi}{\partial \kappa} \mu_a (H_{meas} - H) \quad (20)$$

Integrating over a volume  $V$  with surface  $S$  and assuming  $\partial \Phi / \partial \kappa \rightarrow 0$  on  $S$  as  $S \rightarrow \infty$ , the left-hand side is zero (as above with the absorption case) and we are left with

$$\int \frac{\partial \Phi}{\partial \kappa} \mu_a (H_{meas} - H) dV = - \int \Phi^* \nabla \cdot (\delta(\mathbf{x} - \mathbf{x}_0) \nabla \Phi) dV \quad (21)$$

$$= -\nabla \Phi^* \cdot \nabla \Phi|_{x_0} \quad (22)$$

The functional gradient with respect to  $\kappa$  is therefore

$$\frac{\partial \mathcal{E}}{\partial \kappa} = \nabla \Phi^* \cdot \nabla \Phi \quad (23)$$

As the reduced scattering coefficient  $\mu'_s$  is related to  $\kappa$ , by definition, as  $\kappa = (3(\mu_a + \mu'_s))^{-1}$ , this leads to the relation

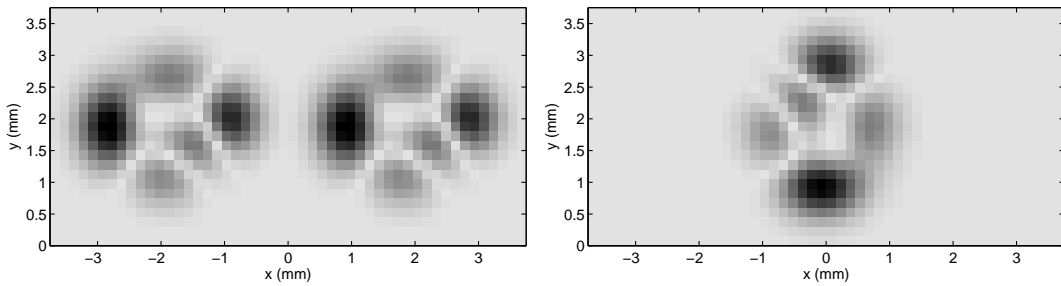
$$\frac{\partial \mathcal{E}}{\partial \mu'_s} = \frac{\partial \mathcal{E}}{\partial \kappa} \frac{\partial \kappa}{\partial \mu'_s} = -3\kappa^2 \frac{\partial \mathcal{E}}{\partial \kappa} \quad (24)$$

and so the functional gradient for the scattering may be written as

$$\boxed{\frac{\partial \mathcal{E}}{\partial \mu'_s} = -3\kappa^2 \nabla \Phi^* \cdot \nabla \Phi} \quad (25)$$

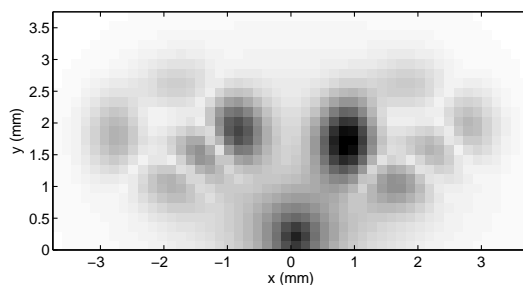
### 2.3. Comparison with Finite Difference Estimation

Figure 1 shows the absorption and scattering coefficient distributions for the  $25 \times 50$  pixel, two-dimensional, examples used in this section. For a pencil beam illuminating this example centrally from below, the absorbed energy density distribution is shown in Fig. 2. In all these examples the 2D finite element model described in references [2] and [3] was used, although with a point source close to the boundary representing the collimated beam.<sup>8</sup> For the inversions in Section 2.4, Gaussian noise at a constant level was added to the simulated measurement  $H_{meas}$ , resulting in an absorbed energy-to-noise ratio of -5 to 40 dB depending on position in the image (because the absorbed energy is spatially varying).



**Figure 1.** Absorption coefficient  $\mu_a$  (greyscale range 0-0.3  $\text{mm}^{-1}$ ) and reduced scattering coefficient  $\mu'_s$  (1-6  $\text{mm}^{-1}$ ).

In order to check that the expressions above for the functional gradients are correct, they were compared to functional gradients calculated using a computationally expensive finite-difference approximation: the absorption coefficient was perturbed at each point in turn by a small amount  $\Delta \mu_a$ , the change in the error functional



**Figure 2.** Absorbed energy density distribution corresponding to the absorption and scattering coefficient distributions in Fig. 1 when illuminated centrally from below by a pencil beam.

$\Delta\mathcal{E}$  was recorded, and a finite difference gradient was calculated as  $\Delta\mathcal{E}/\Delta\mu_a$ . The same procedure was used to estimate the functional gradient for  $\mu'_s$ . Figure 3 shows the functional gradients  $\partial\mathcal{E}/\partial\mu_a$  and  $\partial\mathcal{E}/\partial\mu'_s$ , calculated both by the adjoint method, Eqs. (14) and (25), and the finite difference approximation. Both methods gave similar gradients, suggesting the adjoint method was formulated correctly. The differences for  $\partial\mathcal{E}/\partial\mu'_s$  were due to the finite-difference approximation. The left-hand graph, showing  $\partial\mathcal{E}/\partial\mu_a$ , was plotted using both terms from Eq. (14) (solid line) as well as just the first term (dashed line). There is little difference, suggesting that the adjoint model may not be necessary to estimate  $\partial\mathcal{E}/\partial\mu_a$ .

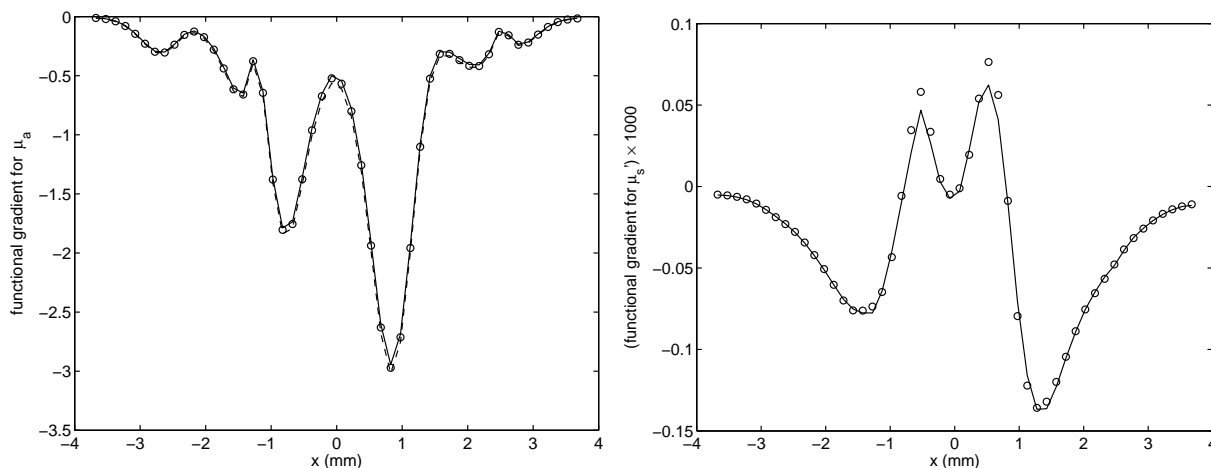


**Figure 3.** (Left graph) The functional gradient  $\partial\mathcal{E}/\partial\mu_a$  along the line  $y = 2$  when the estimate for  $\mu_a = 0.03 \text{ mm}^{-1}$ . The circles have been calculated using a finite-difference approximation, the solid line using Eq. (14), and the dashed line using only the first term from Eq. (14). The dashed line is slightly lower than the solid line. (Right graph) The functional gradient  $\partial\mathcal{E}/\partial\mu'_s$  along the line  $y = 2$  when the estimate for  $\mu'_s$  is 90% of the true value. Circles: finite difference, solid line: Eq. (25).

## 2.4. Separate Inversions for $\mu_a$ and $\mu'_s$

Figure 4 shows the absorption coefficient estimate obtained from the absorbed energy image by using a gradient-based minimisation, when the scattering is known *a priori*. It clearly converges to the true solution, except around the edges where the signal-to-noise ratio is low. Figure 5 shows the reduced scattering coefficient estimate obtained when the absorption coefficient is known *a priori*. It is clearly more affected by the noise in  $H_{meas}$  than the absorption estimate, and convergence soon becomes very slow because of the weaker dependence of the absorbed energy on the scattering. (Unlike  $\mu_a$  which is strongly related to the absorbed energy distribution,  $\mu'_s$  affects it only through the fluence  $\Phi$ .) In both these examples, the Matlab minimisation function `fminunc.m` was used to perform the minimisation. No explicit regularisation was used.

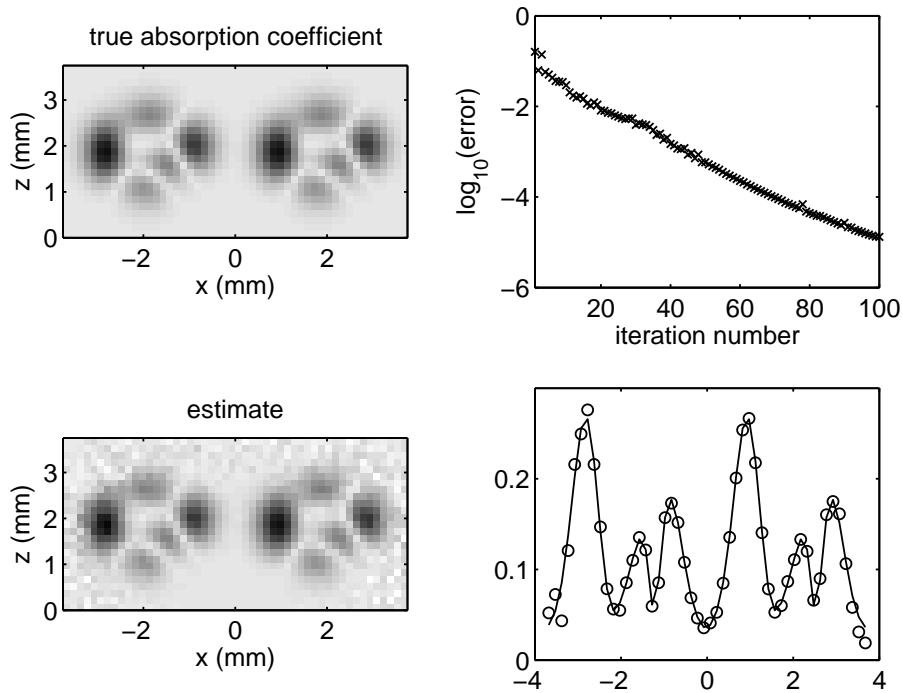


**Figure 4.** Absorption coefficient  $\mu_a$  (greyscale range 0-0.3  $\text{mm}^{-1}$ ) estimated from the absorbed energy image in Fig. 2 from a starting point of  $\mu_a = 0.03 \text{ mm}^{-1}$  everywhere. Top right: log of the error functional  $\mathcal{E}$ . Bottom right: profile of  $\mu_a$  at  $y = 2$  mm, true: solid line, estimated: circles.

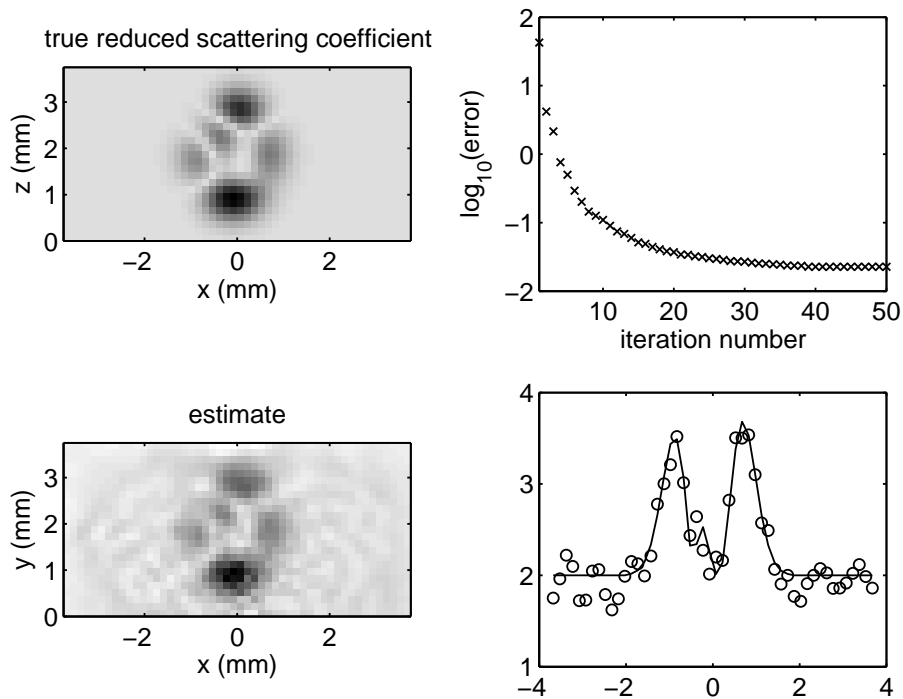


**Figure 5.** Reduced scattering coefficient  $\mu'_s$  (greyscale range 1-6  $\text{mm}^{-1}$ ) estimated from the absorbed energy image in Fig. 2 from a starting point of  $\mu'_s = 1.8 \text{ mm}^{-1}$  everywhere. Top right: log of the error functional  $\mathcal{E}$ . Bottom right: profile of  $\mu'_s$  at  $y = 2$  mm, true: solid line, estimated: circles.

### 3. MULTIWAVELENGTH IMAGING

Estimating both  $\mu_a$  and  $\mu'_s$  from an absorbed energy image obtained at a single wavelength is difficult without some prior knowledge of the solution, such as a positivity condition or smoothness constraint, to reduce the ill-posedness. One way to overcome this nonuniqueness is to use absorbed energy images obtained at multiple wavelengths. Through knowledge of the specific absorption spectra of all the significant chromophores within the sample, and by assuming the wavelength dependence of the scattering is known, the ill-posedness of the inversion can be reduced.<sup>9</sup>

The wavelength-dependent absorption coefficient can be written as a sum of contributions from the major chromophores in the sample under consideration. If  $C_j(\mathbf{x})$  are the concentration distributions of the contributing chromophores and  $\epsilon_j(\lambda)$  are their specific absorption spectra, then the absorption coefficient may be written as

$$\mu_a(\mathbf{x}, \lambda) = \sum_j C_j(\mathbf{x})\epsilon_j(\lambda). \quad (26)$$

The functional gradient for the concentrations can be obtained from the gradient for the absorption through the chain rule

$$\frac{\partial \mathcal{E}}{\partial C_j} = \frac{\partial \mathcal{E}}{\partial \mu_a} \frac{\partial \mu_a}{\partial C_j} = \frac{\partial \mathcal{E}}{\partial \mu_a} \epsilon_j \quad (27)$$

where  $\partial \mu_a / \partial C_j$  has been obtained by differentiating Eq. (26). In tissue, the wavelength-dependence of the scattering often approximates to a power law, allowing the reduced scattering coefficient to be written as

$$\mu'_s = a(\mathbf{x})\lambda^{-b} \quad (28)$$

where  $b$  is constant and all the spatial variation of  $\mu'_s$  is contained in  $a(\mathbf{x})$ . The functional gradient for  $a$  is related to the gradient for the scattering:

$$\frac{\partial \mathcal{E}}{\partial a} = \frac{\partial \mathcal{E}}{\partial \mu'_s} \frac{\partial \mu'_s}{\partial a} = \frac{\partial \mathcal{E}}{\partial \mu'_s} \lambda^{-b} \quad (29)$$

#### 3.1. Inversion for Two Chromophore Distributions

In this final example, the scattering is assumed known, and the concentrations of two different chromophores are estimated from absorbed energy images simulated for four wavelengths using the functional gradient given by Eq. (29). (In fact, this inversion will also converge when as few as two wavelengths are used.) Fig. 6 shows the specific absorption coefficient spectra of the two chromophores. This, along with their concentrations given in Fig. 7, provides the absorption. Simulated absorbed energy images at four wavelengths are shown in Fig. 8. The functional gradients for the two chromophore concentrations were calculated from Eq. (27) and used in a minimisation resulting in the estimates in Fig. 9. The rate at which the minimisation converged to this solution is shown in Fig. 10. It is clear that when the scattering is known, this approach can recover two chromophore distributions. It is worth noting that these distributions are not apparent from the absorbed energy images in Fig. 8 and could not be obtained from them directly. This kind of inversion is of considerable practical interest. For instance, consider a situation in which the absorption of a targeted contrast agent is less than that of an endogenous chromophore, such as hemoglobin, so the distribution of the contrast agent is not clear from the absorbed energy images. In such a case, the approach described here could be used to extract the concentration distribution of the contrast agent from the absorbed energy images despite the presence of the second, endogenous, chromophore.

### 4. SUMMARY

Gradient-based methods for estimating the absorption and scattering coefficient distributions from single-wavelength images, and chromophore concentrations and scattering from multiwavelength images have been proposed. An adjoint method for estimating the functional gradients has been demonstrated. Simple simulated examples were given, in which the absorption or scattering coefficient was estimated when the other was known, and in which two chromophore concentrations were extracted from multiwavelength images. These represent useful steps towards full quantitative photoacoustic imaging. The next step in this research will be to invert for the scattering distribution and several chromophore concentrations simultaneously.

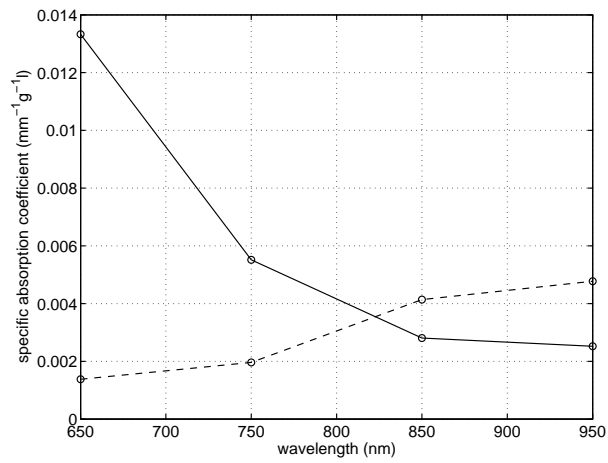


**Figure 6.** Specific absorption spectra of the two chromophores whose concentrations are shown in Fig. 7. Chromophore 1 is has higher absorption at lower wavelengths.

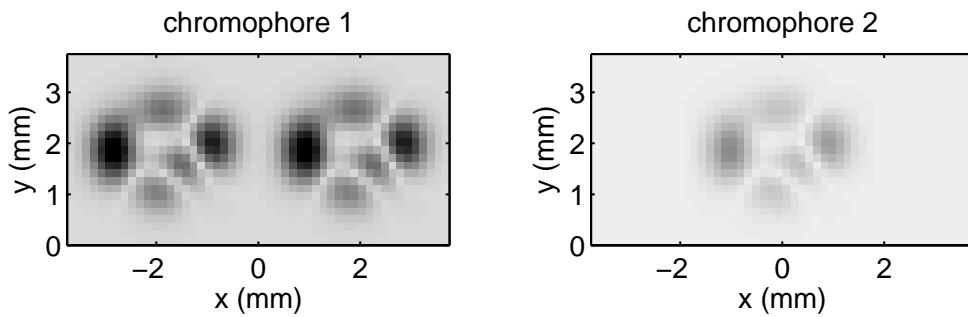


**Figure 7.** The concentration distributions of two chromophores with specific absorption coefficient spectra shown in Fig. 6 (greyscale 0-70  $\text{gl}^{-1}$ ).

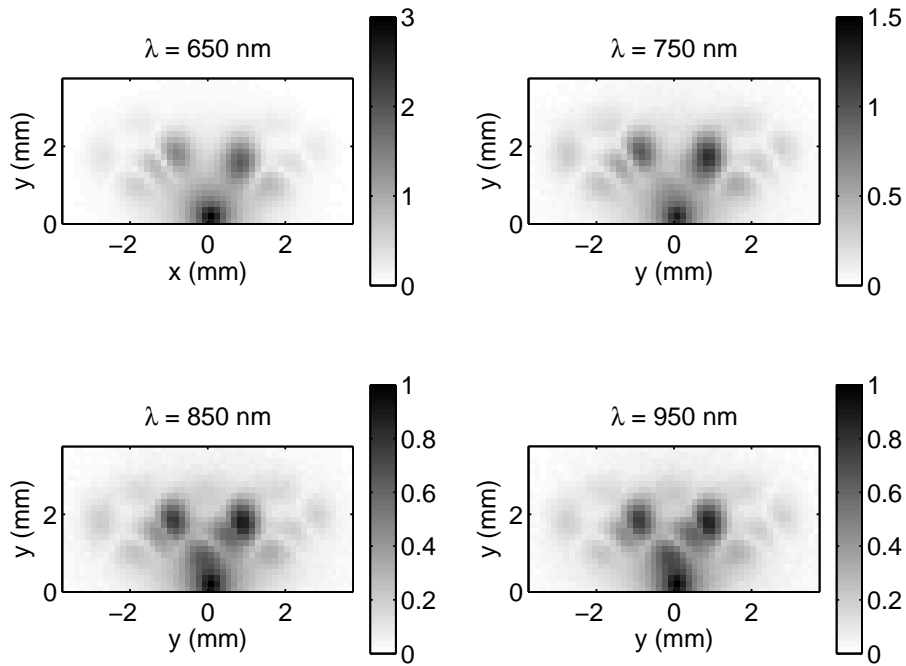


**Figure 8.** Absorbed energy images at four wavelengths. The absorption is due to the two chromophores whose specific absorption spectra and concentrations are shown in Figs. 6 and 7 respectively. In this example  $b = 0$ , and  $\mu'_s$ , which is therefore wavelength-independent, is constant at  $1 \text{ mm}^{-1}$ .

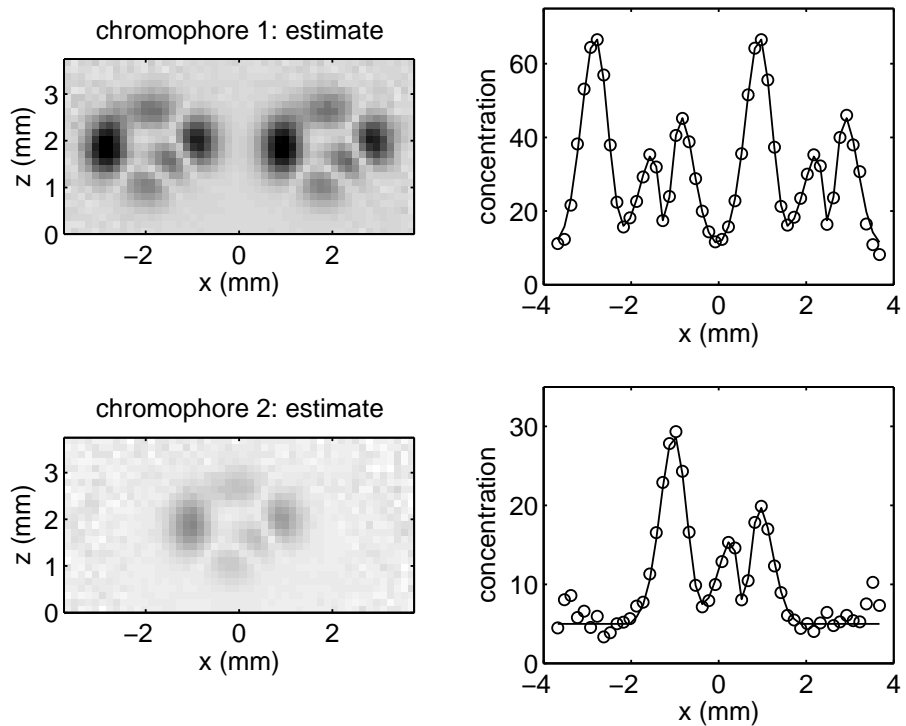


**Figure 9.** Estimates of the two chromophore concentrations shown in Fig. 7, obtained using a gradient-based minimisation (greyscale  $0\text{-}70 \text{ g l}^{-1}$ ). Solid line: true concentration, circles: estimate.

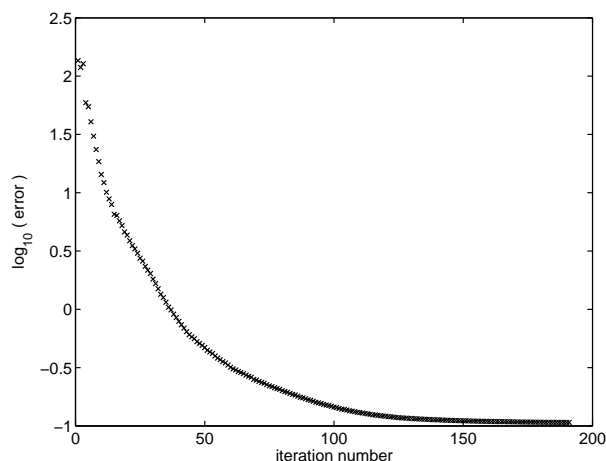


**Figure 10.** The value of the error functional as a function of iteration number for the minimisation resulting in the chromophore concentration estimates shown in Fig. 9.

### ACKNOWLEDGMENTS

This work was supported by the Engineering and Physical Sciences Research Council, UK.

### REFERENCES

1. J. G. Laufer, C. Elwell, D. Delpy, and P. Beard, "Quantitative spatially resolved measurement of tissue chromophore concentrations using photoacoustic spectroscopy: application to the measurement of blood oxygenation and haemoglobin concentration," *Phys. Med. Biol.* **52**, pp. 141–168, 2007.
2. B. T. Cox, S. Arridge, K. Köstli, and P. Beard, "Quantitative photoacoustic imaging: fitting a model of light transport to the initial pressure distribution," *Proc. SPIE* **5697**, pp. 49–55, 2005.
3. B. T. Cox, S. R. Arridge, K. Köstli, and P. C. Beard, "2D quantitative photoacoustic image reconstruction of absorption distributions in scattering media using a simple iterative method," *Appl. Opt.* **45**(8), pp. 1866–1874, 2006.
4. J. G. Laufer, C. Elwell, D. Delpy, and P. Beard, "In vitro measurements of absolute blood oxygen saturation using pulsed near-infrared photoacoustic spectroscopy: accuracy and resolution," *Phys. Med. Biol.* **50**, pp. 4409–4428, 2005.
5. B. T. Cox, S. Arridge, and P. Beard, "Quantitative photoacoustic image reconstruction for molecular imaging," *Proc. SPIE* **6086**, p. 60861M, 2006.
6. Z. Yuan and H. Jiang, "Quantitative photoacoustic tomography: Recovery of optical absorption coefficient maps of heterogeneous media," *App. Phys. Lett.* **88**, p. 231101, 2006.
7. J. Ripoll and V. Ntziachristos, "Quantitative point source photoacoustic inversion formulas for scattering and absorbing media," *Physical Review E* **71**, p. 031912, 2005.
8. M. Schweiger, S. Arridge, M. Hiraoka, and D. Delpy, "The finite element method for the propagation of light in scattering media: Boundary and source conditions," *Medical Physics* **22**, pp. 1779–1792, 1995.
9. A. Corlu, R. Choe, T. Durduran, K. Lee, M. Schweiger, S. Arridge, E. Hillman, and A. Yodh, "Diffuse optical tomography with spectral constraints and wavelength optimization," *Applied Optics* **44**, pp. 2082–2093, 2005.